Deep Very Long Baseline Interferometry Constraints on Compact Radio Cores in Four Ultraluminous X-Ray Sources

The Astrophysical Journal, 1003:118 (7pp), 2026 June 1 https://doi.org/10.3847/1538-4357/ae63cb

Deep Very Long Baseline Interferometry Constraints on Compact Radio Cores in Four Ultraluminous X-Ray Sources

Ailing Wang[1,2], Hua Feng[1], Tao An[3,4], Yijia Zhang[5], Jun Yang[6], Roberto Soria[7,8], Lian Tao[1], Thomas Russell[9], Jing Guo[5], and Liang Zhang[1]
[1] State Key Laboratory of Particle Astrophysics, Institute of High Energy Physics, Chinese Academy of Sciences, Beijing 100049, People's Republic of China; hfeng@ihep.ac.cn
[2] Spallation Neutron Source Science Center, Dongguan 523803, People's Republic of China
[3] Shanghai Astronomical Observatory, Chinese Academy of Sciences, 80 Nandan Road, Shanghai 200030, People's Republic of China
[4] Department of Astronomy, University of Science and Technology of China, Hefei, Anhui 230026, People's Republic of China
[5] Department of Astronomy, Tsinghua University, Beijing 100084, People's Republic of China
[6] Department of Space, Earth and Environment, Chalmers University of Technology, Onsala Space Observatory, SE-439 92 Onsala, Sweden
[7] INAF—Osservatorio Astrofisico di Torino, Strada Osservatorio 20, I-10025 Pino Torinese, Italy
[8] Sydney Institute for Astronomy, School of Physics A28, The University of Sydney, Sydney NSW 2006, Australia
[9] INAF, Istituto di Astrofisica Spaziale e Fisica Cosmica, Via U. La Malfa 153, I-90146 Palermo, Italy
Received 2026 March 17; revised 2026 April 20; accepted 2026 April 21; published 2026 May 20

Abstract

We present high-sensitivity very long baseline interferometry (VLBI) observations of four ultraluminous X-ray sources (ULXs): Holmberg II X-1, IC 342 X-1, NGC 6946 X-1, and NGC 925 X-1. No compact emission was detected on milliarcsecond scales, with rms noise levels reaching approximately 5–20 μJy. The corresponding 5σ flux density upper limits reach $\sim$26 μJy, implying radio luminosity limits $L_R \lesssim 2 \times 10^{33}$ erg s^{-1}. This disfavors any persistently bright hard-state-like compact core at our sensitivity level. The previously reported VLBI core in Holmberg II X-1 exhibits significant long-term variability, broadly consistent with an overall decline over the past decades. This behavior is consistent with emission from optically thin ejecta undergoing adiabatic expansion. The VLBI nondetections may reflect intrinsically weak/intermittent compact emission, and/or low-surface-brightness structure that is resolved out by VLBI, and/or absorption/propagation effects such as free–free absorption in dense, ionized winds.

Unified Astronomy Thesaurus concepts: Ultraluminous x-ray sources (2164); Radio jets (1347); Stellar mass black holes (1611); Very long baseline interferometry (1769)

1. Introduction

Recent observations of ultraluminous X-ray sources (ULXs) suggest that the majority of them are powered by supercritical accretion onto stellar-mass compact objects (for reviews see P. Kaaret et al. 2017; A. King et al. 2023; C. Pinto & D. J. Walton 2023), a physical regime that is not well understood. Numerical simulations involving general relativity have revealed that, besides the massive winds launched due to radiation pressure, supercritical accretion may also drive relativistic jets along the symmetric axis of the accretion flow (A. Sądowski & R. Narayan 2015; Y. Asahina & K. Ohsuga 2024; Y. Zhang et al. 2026). However, the detailed mechanism of jet launch is still controversial.

Observationally, SS 433 remains the most proximate and thoroughly documented archetype of a compact object undergoing supercritical accretion, distinguished by its well-characterized relativistic ($v \approx 0.26c$) jets (K. M. Blundell & M. G. Bowler 2004; S. Fabrika 2004; R. M. Jeffrey et al. 2016). It displays a pair of precessing, relativistic jets with a flux density of about $\sim$1 Jy at the core (at the arcsecond scale) and a mechanical power of about 10^{39} erg s^{-1}. Its binary core has an X-ray luminosity of only $\sim 10^{34-35}$ erg s^{-1} (S. Migliari et al. 2005), but that is because we are looking at the system almost edge-on, and most of the X-ray photons from the central engine are absorbed or blocked by the thick disk and outflows, along our line of sight. If we looked at SS 433 pole-on, it would likely appear to us as a ULX (S. N. Fabrika et al. 2021; M. J. Middleton et al. 2021). The jets, after interacting with the interstellar medium, power the surrounding radio nebula W50, which has a total flux density of 71 Jy at 1.4 GHz and a physical size of $\approx 100 \times 200$ pc (G. M. Dubner et al. 1998) at a distance of 5 kpc (Y. Su et al. 2018).

This raises fundamental questions in accretion physics: whether supercritical accretion can drive collimated, relativistic jets in addition to broad disk outflows; and in what situations jets and outflows coexist. Addressing these requires radio observations of ULXs to search for signatures of jets. In a number of well-studied ULXs, radio observations have revealed optically thin, extended radio emission around them, spatially coincident with the optical emission-line nebula, due to shock ionization by outflows from the central source or photoionization in a few cases (S. D. van Dyk et al. 1994; C. Lacey et al. 1997; N. A. Miller et al. 2005; C. C. Lang et al. 2007; D. Cseh et al. 2012; R. Urquhart et al. 2018; C. T. Berghea et al. 2020; R. Soria et al. 2021; T. Beuchert et al. 2024). However, it is unclear whether the outflow is due to relativistic jets or wide-angle winds. NGC 7793 S26 shows a pair of lobes seen in X-ray, optical, and radio, with a morphology similar to that of W50, seemingly in favor of the jet scenario (T. G. Pannuti et al. 2002; M. W. Pakull et al. 2010; R. Soria et al. 2010). Another SS 433–like system is the microquasar NGC 300 S10, which shows strong evidence for a collimated jet with an estimated power of $\sim 10^{39}$ erg s^{-1}, while

its apparent X-ray luminosity is relatively low, likely because the central emission is absorbed/scattered for a near edge-on geometry (R. Urquhart et al. 2019). Holmberg II X-1 displays a triple radio structure (D. Cseh et al. 2014), with the central component being optically thin, resolved (0.26 pc), and variable (D. Cseh et al. 2015a), reminiscent of collimated jets. Very long baseline interferometry (VLBI) observations of ULXs have identified unresolved compact radio cores in a few cases (M. Mezcua & A. P. Lobanov 2011; M. Mezcua et al. 2013). The high radio flux of those cores suggests an alternative interpretation of those sources as sub-Eddington (low/hard state) intermediate-mass black holes (IMBHs) or low-mass active galactic nuclei (AGN) according to the fundamental plane relations (M. Mezcua et al. 2013). Sporadic or episodic radio activity has been most clearly reported in the transient ULX in M31 (M. J. Middleton et al. 2013) and the IMBH candidate ESO 243-49 HLX-1 (N. Webb et al. 2012; D. Cseh et al. 2015a).

Therefore, it is highly interesting to perform high-sensitivity radio observations of ULXs with VLBI techniques. Detection of compact radio cores will be strong evidence in favor of the jet scenario and may help us distinguish between the observational properties of jet cores in the low/hard state and in the super-Eddington regime (A. Merloni et al. 2003). In this work, we report VLBI observations of four ULXs (Section 2). The observations, data reduction, and results are elaborated in Section 3 and discussed in Section 4. Brief conclusions are presented in Section 5.

2. Targets

We observed Holmberg II X-1, IC 342 X-1, NGC 6946 X-1, and NGC 925 X-1, which are ULXs with a known radio counterpart. These sources have previously been detected at radio wavelengths with the Karl G. Jansky Very Large Array (VLA) and the European VLBI Network (EVN), including reports of compact core candidates or clearly resolved radio structures or nebulae. They therefore represent the most suitable targets for deeper, higher-resolution VLBI observations aimed at testing the presence of compact jet cores on milliarcsecond (mas) scales.

2.1. Holmberg II X-1

Holmberg II X-1 ($d = 3.1$ Mpc; L. Ferrarese et al. 2000) is surrounded by an optical emission-line nebula powered by photoionization (M. W. Pakull & L. Mirioni 2002; P. Kaaret et al. 2004; I. Lehmann et al. 2005). An extended (tens of parsecs) radio nebula with a steep spectrum was found to be spatially consistent with the optical nebula (N. A. Miller et al. 2005; D. Cseh et al. 2012). VLA A-configuration imaging resolved the arcsecond-scale emission into a triple morphology consisting of a central component plus two fainter outer components aligned roughly along the same axis (D. Cseh et al. 2014). A quasi-simultaneous EVN and VLA campaign detected faint, marginally resolved emission at 1.6 GHz but no 5 GHz core down to tens of μJy (D. Cseh et al. 2015b), favoring optically thin synchrotron emission from discrete ejecta (or hotspots) rather than a persistent, compact, self-absorbed flat-spectrum jet base.

2.2. IC 342 X-1

IC 342 X-1 ($d = 3.3$ Mpc; A. Saha et al. 2002) is associated with a shock-ionized optical "tooth" nebula (M. W. Pakull & L. Mirioni 2002; T. P. Roberts et al. 2003), and also an extended radio counterpart interpreted as optically thin synchrotron emission (D. Cseh et al. 2012). At the IC 342 X-1 position, the radio flux density is $\sim$90 μJy, but this is likely contaminated or even dominated by the nebula emission. Previous EVN observations at 1.6 GHz yielded a nondetection of any milliarcsecond-scale core (<35 μJy at 5σ; D. Cseh et al. 2012). Subsequent VLA monitoring likewise did not detect any emission at a similar sensitivity (H. Marlowe et al. 2014).

2.3. NGC 6946 X-1

NGC 6946 X-1 ($d = 7.7$ Mpc; G. S. Anand et al. 2018) resides in the optical nebula MF16, which is argued to be powered by both shock and photoionization (W. P. Blair et al. 2001; P. Abolmasov 2008). Arcsecond-resolution VLA imaging finds mJy-level flux densities at GHz frequencies, with a steep spectrum and an extended morphology coincident with the optical nebula (C. Lacey et al. 1997; T. Beuchert et al. 2024).

2.4. NGC 925 X-1

NGC 925 X-1 ($d = 9.3$ Mpc; A. Saha et al. 2006) is spatially coincident with an optical emission-line nebula possibly due to X-ray irradiation (M. Heida et al. 2016; M. A. Lara-López et al. 2021). Recently, a radio counterpart was reported by matching the ULX position with Very Large Array Sky Survey (VLASS) and Rapid ASKAP Continuum Survey (RACS) images (Y. Zhang et al. 2026). The radio emission is unresolved with the survey data, showing a flux density of 0.6 mJy at 3 GHz with a steep spectral index of -1.1.

In sum, previous observations have shown evidence that the four ULXs may have powerful jets or winds, being good candidates for our VLBI observations.

3. Data Reduction and Results

We observed Holmberg II X-1, IC 342 X-1, and NGC 6946 X-1 with the National Radio Astronomy Observatory (NRAO) Very Long Baseline Array (VLBA) in 2024–2025 (programs BF135, BF137; Table 1). Each session lasted 6 hr and was conducted at L-band (central frequency $\simeq$1.6 GHz) and C-band (central frequency $\simeq$6.2 GHz). We observed NGC 925 X-1 at the L band with both the EVN (program EZ035) and the VLBA (program BZ116; Table 1). The VLBA observations used dual circular polarization with 2-bit sampling at a recording rate of 4 Gbps, configured as four 128 MHz intermediate frequencies (IFs; total bandwidth 512 MHz per polarization). The EVN observations were conducted with eight antennas, using four IFs with 32 MHz bandwidth each, four polarizations, 64 spectral channels per sub-band, and 2 s integrations.

Because ULXs are intrinsically faint at milliarcsecond scales, we employed phase referencing using a 5 minute nodding cycle (1 minute on the phase calibrator and 4 minutes on target). The phase calibrators are listed in Table 1. Most epochs used the full 10-antenna VLBA array, with the few antenna dropouts noted in Table 1.

Table 1
VLBA and EVN observation logs

Obs. Date	Source	Freq. (GHz)	Code	$B_{maj} \times B_{min}$, B_{PA} (mas × mas, deg)	rms (μJy beam^{-1})	$\log \frac{L_R}{erg}$ s^{-1}	Calibrator
(1)	(2)	(3)	(4)	(5)	(6)	(7)	(8)
2024-11-26	Holmberg II X-1	6.2	BF135AC	3.0 × 1.7, −21	10	<33.55	J0831+7035
2024-12-02	Holmberg II X-1	6.2	BF135BC	2.5 × 1.3, −18	9.1	<33.51	J0831+7035
2024-12-06	Holmberg II X-1	6.2	BF135CC	2.5 × 1.3, −18	8.9	<33.50	J0831+7035
2024-12-09	Holmberg II X-1	6.2	BF135DC	2.5 × 1.3, −20	8.8	<33.50	J0831+7035
Stack	Holmberg II X-1	6.2	BF135C	2.5 × 1.3, −19	5.2	<33.27	J0831+7035
2024-12-18	Holmberg II X-1	1.6	BF135AL	9.7 × 5.1, −8.0	17	<33.19	J0831+7035
2025-01-02	Holmberg II X-1	1.6	BF135BL	9.8 × 5.0, −22	19	<33.24	J0831+7035
2025-01-08	Holmberg II X-1	1.6	BF135CL	9.9 × 5.0, −22	17	<33.19	J0831+7035
2025-01-10	Holmberg II X-1	1.6	BF135DL	8.7 × 4.7, −16	25	<33.36	J0831+7035
Stack	Holmberg II X-1	1.6	BF135L	9.5 × 5.1, −16	8.6	<32.90	J0831+7035
2025-02-11	IC 342 X-1	1.6	BF137L1	9.6 × 5.0, −8.4	18	<33.27	J0344+6827
2025-02-14	IC 342 X-1	6.2	BF137C1	3.8 × 2.8, −20	13	<33.72	J0344+6827
2025-03-22	NGC 6946 X-1	1.6	BF137L4	11 × 5.6, −16	19	<34.03	J2035+5821
2025-03-21	NGC 6946 X-1	6.2	BF137C4	2.6 × 1.3, −8.5	10	<34.34	J2035+5821
2025-04-09	NGC 925 X-1	1.7	EZ035	6.2 × 2.2, 3.9	17	<34.18	J0226+3421
2025-08-11	NGC 925 X-1	1.6	BZ116	14 × 4.6, −6.1	21	<34.24	J0226+3421

Notes. Columns: (1) observation date, (2) source name, (3) frequency in GHz, (4) project code, (5) beam size and position angle, (6) off-source image rms noise measured in a nearby source-free region, (7) 5σ luminosity upper limit, and (8) calibrator.
Overall, the VLBA observations were carried out with the standard array of BR, FD, HN, KP, LA, MK, NL, OV, PT, and SC, with KP missing in BF135DL, MK missing in BF137C1, SC missing in BF137L4, and BR missing in BZ116, while all other epochs used a complete or nearly complete VLBA antenna configuration. There are eight stations in EVN observation, including Jb, Wb, Ef, O8, T6, Tr, Hh, and Ir.

Correlation was performed with the Distributed FX (DiFX) software correlator at the VLBA correlator in Socorro (A. T. Deller et al. 2011) and the EVN software correlator SFXC at the Joint Institute for VLBI ERIC (JIVE; A. Keimpema et al. 2015), which minimizes time and bandwidth smearing over the region imaged around each ULX. The correlated data were transferred to the China Square Kilometre Array Regional Centre (T. An et al. 2019, 2022) for calibration and imaging.

VLBA calibration followed standard VLBA procedures in the Astronomical Image Processing System (AIPS; E. W. Greisen 2003). We applied a priori amplitude calibration using measured system temperatures and gain curves (ANTAB and APCAL). Dispersive ionospheric delays were corrected with TECOR using total electron content maps from the NASA CDDIS archive, and Earth-orientation parameters were updated using CLCOR. Parallactic-angle corrections were applied with VLBAPANG. Instrumental phase and delay offsets between IFs were corrected using pulse-cal signals (VLBAMPCL), and residual multiband delays and rates were solved by global fringe fitting on the phase calibrators (FRING). We also derived complex bandpass solutions (BPASS) and applied them before imaging.

EVN calibration was performed in AIPS following standard EVN VLBI procedures. Instrumental phase and delay offsets between IFs were corrected using fringe fitting on strong calibrators. Residual multiband delays, delay rates, and time-dependent phases were then solved by global fringe fitting on the phase calibrators, with the solutions transferred to the target source. Complex bandpass responses were derived from a dedicated bandpass calibrator and applied to the data (BPASS). Where necessary, instrumental delay and fringe-fitting steps were repeated after bandpass calibration to remove any residual sub-band offsets. The fully calibrated data were subsequently used for imaging and further analysis.

We imaged the phase calibrators in DIFMAP (M. C. Shepherd et al. 1994) and iterated CLEAN and self-calibration to refine calibrator structure models; the resulting solutions were transferred back to AIPS and applied to the target datasets. Targets were imaged in Stokes I using natural weighting to maximize point-source sensitivity, and we additionally generated (u, v)-tapered images to search for partially resolved emission. Because none of the ULXs are detected, no self-calibration was performed on the targets.

For Holmberg II X-1, we concatenated the four epochs at each band using DBCON to improve image sensitivity. The final synthesized beams and rms noise levels are listed in Table 1.

We imaged each epoch at each frequency using natural weighting to maximize point-source sensitivity and also produced a set of (u, v)-tapered images to increase sensitivity to low-surface-brightness emission on the largest VLBA-resolved scales. No compact emission is detected at the ULX positions, nor elsewhere within the imaged fields, at either frequency in any epoch. We adopt point-source upper limits of $S_{\nu,\rm lim} = 5\sigma_{\rm rms}$, where $\sigma_{\rm rms}$ is measured in a nearby source-free region. The corresponding upper limits in radio luminosity are also computed as $L_R \equiv \nu L_\nu$ assuming the source distance, also listed in Table 1.

4. Discussion

Our VLBI observations yielded nondetections of the four ULXs, allowing us to place stringent upper limits (down to several tens of μJy at 5σ) on any compact milliarcsecond-scale core emission, and more generally on any milliarcsecond-scale jet/lobe-like structure with sufficiently high surface brightness. More extended, low-surface-brightness emission on subarcsecond/arcsecond scales would be resolved out by VLBI and is not constrained by these limits. Here we discuss the possible physical nature in line with the nondetections.

Table 2
Radio Flux Densities and Upper Limits of the Holmberg II X-1

Telescope	Beam Size (arcsec × arcsec)	Obs. Date	Freq. (GHz)	Flux Density (mJy)	References
(1)	(2)	(3)	(4)	(5)	(6)
VLA	1.7 × 1.5	1988,1989,1990,1991	4.9	0.677± 0.207	1
VLA	1.9 × 1.5	1994-04-03	1.4	1.174 ± 0.085	1
VLA	1.5 × 1.0	2007-12-08	4.8	0.114±0.014	2
VLA	2.4 × 1.8	2008-04-21	8.5	0.145±0.015	2
VLA	0.41 × 0.30	2012-12-16/17	5.0	0.151±0.003	3
EVN	0.012 × 0.010	2014-01-14	1.6	0.053±0.015	4
EVN	0.003 × 0.002	2014-04-28	5.0	<0.060	4
VLA	0.41 × 0.22	2014-05-25	9.0	0.015±0.007	4
VLASS	3.4 × 2.0	2017-09-18	3.0	<0.803	5
VLASS	3.3 × 2.1	2020-09-10	3.0	<0.778	5
VLASS	3.4 × 2.3	2023-02-17	3.0	<0.605	5
VLBA	0.0025 × 0.0013	2024-11-26 to 2024-12-09	6.2	<0.026	this work
VLBA	0.0095 × 0.0051	2024-12-18 to 2025-01-10	1.6	<0.043	this work
VLASS	3.2 × 2.0	2026-01-02	3.0	<0.640	5

Notes. Columns: (1) telescope, (2) beam size, (3) observing date, (4) frequency, (5) flux density or 5σ upper limit, and (6) references.
References. (1) N. A. Miller et al. (2005); (2) D. Cseh et al. (2012); (3) D. Cseh et al. (2014); (4) D. Cseh et al. (2015b); (5) M. Lacy et al. (2020).

4.1. Comparison with X-Ray Binaries

Adopting the measured flux upper limits, the beam-averaged brightness-temperature limits can be expressed as

$$T_b < 1.22 \times 10^{12} \left(\frac{S_{\nu,\mathrm{lim}}}{\mathrm{Jy}}\right)\left(\frac{\nu}{\mathrm{GHz}}\right)^{-2}\left(\frac{\theta_{\mathrm{maj}}\theta_{\mathrm{min}}}{\mathrm{mas}^2}\right)^{-1} \quad \mathrm{K}\,, \quad (1)$$

where θ_{maj} and θ_{min} are the beam size along the major and minor axes, respectively. Given the deepest stacked observations of Holmberg II X-1 (Table 1) as an example, one obtains $T_b < 3 \times 10^5$ K at 6.2 GHz and $T_b < 4 \times 10^5$ K at 1.6 GHz. These values are lower than the brightness temperatures typically reported for bright hard-state compact cores in black hole X-ray binaries (e.g., $T_B > 10^6$ K; V. Dhawan et al. 2000; A. M. Stirling et al. 2001; J. C. A. Miller-Jones et al. 2009; Z. Paragi et al. 2013), noting that our limits are beam averaged and thus primarily constrain the surface brightness on milliarcsecond scales.

These limits primarily constrain the milliarcsecond-scale surface brightness. They therefore disfavor any persistently bright, Doppler-boosted compact core at our achieved sensitivity, but they do not by themselves exclude intrinsically high-T_b emission confined to angular scales $\ll$ the synthesized beam if the total flux density is below our detection thresholds, nor do they rule out low-surface-brightness structure distributed on larger scales that would be resolved out by VLBI. Consequently, the present nondetections indicate that none of the four ULXs show a stable, bright VLBI core during the observed epochs, rather than uniquely requiring a complete absence of compact jet activity.

If SS 433 were placed at 3.1 Mpc, a 2.5 mas VLBA beam would correspond to a physical scale of ≈0.038 pc, equivalent to $\approx 1\farcs6$ at the distance of SS 433 (∼5 kpc). This is comparable to the extent of the central core region detected with the VLA with a 5 GHz radio luminosity $\nu L_\nu \sim 10^{32}$ erg s^{-1} (A. M. Stirling et al. 2004). Its core flux density at 3.1 Mpc would drop to ∼2 μJy. Our VLBA limits therefore do not exclude SS 433–like jets if their compact radio cores are as faint at GHz frequencies as implied by the SS 433 scaling. However, we note that the outflow mechanical power estimated from shock-ionized nebulae in ULXs is generally 1 or 2 orders of magnitude higher than that in SS 433 (M. W. Pakull & L. Mirioni 2002).

4.2. Temporal Variability

The EVN observation on 2014 January 14 detected a flux density of 53 ± 15 μJy at 1.6 GHz from Holmberg II X-1 (D. Cseh et al. 2015b), while our 3σ upper limit is 25.8 μJy and 5σ upper limit is 43 μJy at the same band with similar beam sizes. The two measurements are inconsistent with each other at a significance greater than 3σ, suggesting that the radio emission is transient or variable at the VLBI scale. In particular, D. Cseh et al. (2015b) revealed that the radio core is extended on milliarcsecond scale with unboosted emission, and faded by a factor of 7.3 or more over the course of 1.5 yr, eventually falling below the detection threshold in later epochs, which is compatible with the scenario of adiabatic expansion. Along with the steep spectrum ($\alpha = -0.8$; D. Cseh et al. 2014), the central core is more likely an ejecta rather than a compact steady jet.

We compiled published VLA, EVN, VLBA, and VLASS measurements for the central radio region of Holmberg II X-1 in Table 2 and show them in Figure 1 after scaling them to 5 GHz assuming $\alpha = -0.8$ for illustrative comparison. We emphasize, however, that this spectral index was inferred from a limited set of earlier measurements and should not be regarded as a time-independent property of the source. Given the known variability of Holmberg II X-1, the spectral index may also vary with epoch and source state, and free–free absorption at lower frequencies could further affect the spectral shape and hence the extrapolated fluxes. We also caution that the compiled measurements span a wide range of angular resolutions, from milliarcsecond-scale EVN/VLBA data to subarcsecond and arcsecond-scale VLA/VLASS observations. The lower-resolution measurements may therefore include significant contributions from expanding ejecta and/or emission from the surrounding ionized nebula, rather than isolating the compact core alone. Taken together, the available data are broadly consistent with long-term variability, and possibly fading central radio emission, but they do

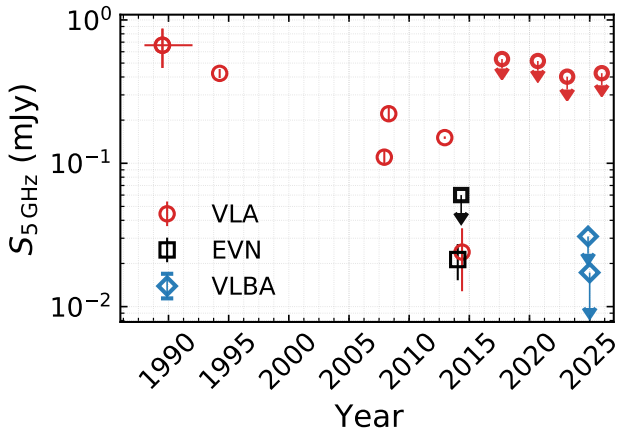

Figure 1. Radio light curve of Holmberg II X-1 at 5 GHz. Compilation of published radio measurements and upper limits for the central radio region of Holmberg II X-1, scaled to 5 GHz assuming a power-law spectral index $\alpha = -0.8$ (D. Cseh et al. 2014) for illustrative comparison. Red circles show VLA measurements, black squares show EVN measurements, and blue diamonds show VLBA measurements (Table 2). Downward triangles denote upper limits for nondetections. The early VLA measurements obtained between 1988 and 1991 are shown as a single point at the midpoint epoch (1989.5), with the horizontal error bar indicating the full time span of the observations. The compiled measurements span a wide range of angular resolutions; different data points likely include different amounts of extended (noncore) emission (Table 2).

not uniquely establish a monotonic decline of an isolated compact core. This ambiguity further strengthens the case for sensitive VLBI monitoring of ULXs, which is essential for disentangling any genuine compact core from nearby ejecta/bolides and more extended nebular emission.

Sporadic or episodic radio activity has been seen in two ULXs: a transient ULX in M31 (M. J. Middleton et al. 2013) and ESO 243-49 HLX-1 (N. Webb et al. 2012; D. Cseh et al. 2015a). However, these two ULXs show distinct X-ray behaviors from canonical ULXs like the four in this work. Most ULXs have been active since they were discovered in the 1980s with the Einstein telescope, while the M31 transient was in the outburst for less than a year (M. J. Middleton et al. 2013), and HLX-1 has been in quiescence after several cycles of outbursts (or large amplitude variation) since its discovery (L. C.-C. Lin et al. 2020). HLX-1 shows intermittent, short-lived transient radio detections during X-ray outbursts, especially around the hard-to-soft state transition. ATCA detected tens of μJy emission at 5 and 9 GHz that disappeared in adjacent epochs, and the strong variability favors discrete jet ejection events rather than a steady core (N. Webb et al. 2012; D. Cseh et al. 2015a). These ejecta are expected when an X-ray binary transitions from the hard to soft state (R. P. Fender et al. 2004, 2009), while other ULXs are not staying at any of these sub-Eddington spectral states (M. J. Middleton et al. 2015).

4.3. Absorption in the Close Vicinity

The majority of ULXs are high-mass X-ray binaries at the high-luminosity end (S. Mineo et al. 2012). Population studies suggest that they may contain an evolved companion (N. Madhusudhan et al. 2008). A B9Ia supergiant was identified in NGC 7793 P13 (C. Motch et al. 2014), and a helium star was identified in NGC 247 X-1 (C. Zhou et al. 2023). Also, massive disk winds are believed to be ubiquitous in supercritical accretion, as suggested by theory (D. L. Meier 1982; J. Poutanen et al. 2007) and supported by observations (S. Fabrika et al. 2015; Y. Zhou et al. 2019; Y. Qiu & H. Feng 2021). Thus, ULXs may be embedded in an environment filled with stellar and/or disk winds.

For a spherically symmetric ionized wind with mass-loss rate $\dot{M}$ and terminal speed v, the electron density scales as $n_e(r) \propto \dot{M}\, r^{-2} v^{-1}$, and the emission measure scales as $\mathrm{EM} \propto \dot{M}^2 v^{-2} R_0^{-3}$, where R_0 is the launching radius of the wind. Using the standard approximation,

$$\tau_{\mathrm{ff}} \simeq 0.082 \left(\frac{T_e}{\mathrm{K}}\right)^{-1.35} \left(\frac{\nu}{\mathrm{GHz}}\right)^{-2.1} \left(\frac{\mathrm{EM}}{\mathrm{pc\ cm^{-6}}}\right), \tag{2}$$

and adopting the representative wind velocity and temperature for ULXs detected with ionized winds (C. Pinto et al. 2016), one obtains

$$\tau_{\mathrm{ff}}(6\ \mathrm{GHz}) \approx 0.53 \left(\frac{\dot{M}}{10^{-4}\, M_\odot\ \mathrm{yr^{-1}}}\right)^2 \left(\frac{v}{0.1c}\right)^{-2} \times \left(\frac{T_e}{10^7\ \mathrm{K}}\right)^{-1.35} \left(\frac{R_0}{10^{13}\ \mathrm{cm}}\right)^{-3}. \tag{3}$$

Here we assume that ULXs have a mass-loss rate comparable to that of SS 433 (S. Fabrika 2004) and a launching radius (i.e., the inner boundary of the absorbing screen) comparable to the binary separation. Under these representative parameters, free–free optical depths of order unity at 6 GHz (and substantially larger at 1.6 GHz) are possible for supercritical mass-loss rates and sufficiently small R_0. In that case, free–free absorption could contribute to suppressing the apparent GHz-band VLBI core flux (in particular for the cases of IC 342 X-1, NGC 6946 X-1, and NGC 925 X-1), although the present nondetections can equally be explained by intrinsically weak/intermittent compact emission and/or low-surface-brightness structure that is resolved out by VLBI. High-frequency VLBI ($\gtrsim$15 GHz), where τ_{ff} is expected to decrease rapidly with frequency, would provide an effective test of this scenario. Such observations, if yielding detections, would also help place useful constraints on the circumsource environment of ULXs and, consequently, on their accretion physics and/or evolutionary history.

4.4. Fundamental Plane and IMBH Interpretation

The radio upper limits derived in this work cannot exclude the possibility that the four ULXs follow the radio–X-ray luminosity correlation found for hard-state X-ray binaries (S. Corbel et al. 2013; K. I. I. Koljonen & D. M. Russell 2019). If a ULX were a sub-Eddington, hard-state accretor with a scale-invariant compact jet, its core radio luminosity should follow

$$\log L_R = 0.60 \log L_X + 0.78 \log M_{\mathrm{BH}} + 7.33, \tag{4}$$

where $L_R \equiv \nu L_\nu$ at 5 GHz and L_X is the 2–10 keV luminosity (A. Merloni et al. 2003). Under this assumption, our VLBA limits can be translated into upper limits on M_{BH}. Approximating our 6.2 GHz limits as 5 GHz limits for a flat core spectrum, we obtain $M_{\mathrm{BH}} \lesssim 3.1 \times 10^2 L_{\mathrm{X},40}^{-0.77} M_\odot$ (Holmberg II X-1), $M_{\mathrm{BH}} \lesssim 1.2 \times 10^3 L_{\mathrm{X},40}^{-0.77} M_\odot$ (IC 342 X-1), and $M_{\mathrm{BH}} \lesssim 7.2 \times 10^3 L_{\mathrm{X},40}^{-0.77} M_\odot$ (NGC 6946 X-1), where $L_{X,40}$ is $L_X/(10^{40}\ \mathrm{erg\ s^{-1}})$. For context, the fundamental-plane-based constraints reported for ULXs typically fall in the IMBH regime, with representative values ranging from

$M_{\rm BH} \lesssim (1.0 \pm 0.3) \times 10^3\,M_\odot$ (IC 342 X-1, D. Cseh et al. 2012) to $\log(M_{\rm BH}/M_\odot) < 4.2$–5.9 for several systems (M. Mezcua et al. 2013), whereas HLX-1 allows $M_{\rm BH} \lesssim 2.8 \times 10^6\,M_\odot$ (D. Cseh et al. 2014) and M82 X-1 has $\sim 2.7 \times 10^3\,M_\odot$ with large uncertainties (D. Williams-Baldwin et al. 2025). These limits should be interpreted with caution because ULXs usually occupy the ultraluminous regime rather than canonical hard states (e.g., J. C. Gladstone et al. 2009), where the fundamental plane has not been tested. The inflow–outflow coupling and accretion geometry in ULXs may differ substantially from those of the systems on which the fundamental plane is based. Plus, the radio and X-ray luminosities were not measured simultaneously, which introduces additional uncertainties. However, any future secure radio detection of these sources at VLBI resolution could imply the presence of an IMBH (e.g., T. Panurach et al. 2024).

4.5. Super-Eddington Feedback as a Generic Astrophysical Process

Beyond ULXs, the central question probed here, *how supercritical accretion partitions energy between radiation, winds, and jets*, is of broad relevance to compact-object feedback across the mass scale. ULXs are among the best nearby laboratories for the physics that is invoked in models of rapid black hole growth and feedback in dense environments. Our results strengthen a picture in which the time-averaged mechanical impact of supercritical accretion can be large, while the instantaneous compact jet core may be radio weak or hidden. This decoupling has direct implications for interpreting VLBI nondetection of the compact radio component in other high-Eddington systems and for designing future multiwavelength campaigns aimed at catching the intermittent, potentially transition-linked radio episodes expected if discrete ejecta occur.

5. Conclusions

We have performed high-sensitivity VLBI observations of four ULXs, Holmberg II X-1, IC 342 X-1, NGC 6946 X-1, and NGC 925 X-1, to search for milliarcsecond-scale radio emission.

No compact emission is detected in any dataset, with a 5σ upper limit as deep as 26 μJy at 6.2 GHz for Holmberg II X-1. For the other sources, the 5σ flux-density upper limits are at the level of $\sim$50–100 μJy. These correspond to core radio-power limits of $L_R < (1.6 - 22) \times 10^{33}$ erg s^{-1}. These upper limits, together with the beam sizes, can be translated to brightness temperatures no more than a few times 10^5 K in both bands, lower than the beam-averaged brightness temperatures typically inferred for bright hard-state compact cores, while primarily constraining milliarcsecond-scale surface brightness.

For Holmberg II X-1, its central radio emission is found to be highly variable. Overall, it has shown a declining trend over the past 35 yr, consistent with the scenario that it is optically thin ejecta undergoing adiabatic expansion.

Another possibility is that the nondetections are actually due to free–free absorption in the vicinity of the binary system, as the binary system may be immersed in dense, ionized winds. Future high-frequency VLBI observations may test this scenario and place physical constraints on the accretion physics and/or evolutionary history.

Acknowledgments

We thank the referee for the careful reading of the manuscript and for the constructive comments and suggestions, which helped improve the quality and clarity of this work. H.F. acknowledges funding support from the National Natural Science Foundation of China under grant 12025301, the Strategic Priority Research Program of the Chinese Academy of Sciences, and China's Space Origins Exploration Program. A.W. is supported by the National Natural Science Foundation of China under grant No. 12503018 and the China Postdoctoral Science Foundation under grant Nos. 2025M773197 and 2025T180874. This work is supported by the National SKA Program of China (grant No. 2022SKA0120102). T.A. acknowledges support from Shanghai Oriental Talent Project, the Xinjiang Tianchi Talent Program, and the FAST Special Program (NSFC 12041301). The VLBI data processing made use of the computing resource of the China SKA Regional Centre (T. An et al. 2019, 2022). The National Radio Astronomy Observatory is a facility of the National Science Foundation operated under cooperative agreement by Associated Universities, Inc. Scientific results from data presented in this publication are derived from VLBA project codes BF135, BF137, and BZ116, and EVN project code EZ035.

Facilities: EVN, VLBA.

Software: astropy (Astropy Collaboration et al. 2013, 2018), AIPS (E. W. Greisen 2003), Difmap (M. C. Shepherd et al. 1994).

ORCID iDs

Ailing Wang https://orcid.org/0000-0002-7351-5801
Hua Feng https://orcid.org/0000-0001-7584-6236
Tao An https://orcid.org/0000-0003-4341-0029
Yijia Zhang https://orcid.org/0009-0008-8549-8069
Jun Yang https://orcid.org/0000-0002-2322-5232
Roberto Soria https://orcid.org/0000-0002-4622-796X
Lian Tao https://orcid.org/0000-0002-2705-4338
Thomas Russell https://orcid.org/0000-0002-7930-2276
Jing Guo https://orcid.org/0000-0001-9346-3677
Liang Zhang https://orcid.org/0000-0003-4498-9925

References

Abolmasov, P. 2008, AIPC, 1054, 33
An, T., Wu, X., Lao, B., et al. 2022, SCPMA, 65, 129501
An, T., Wu, X.-P., & Hong, X. 2019, NatAs, 3, 1030
Anand, G. S., Rizzi, L., & Tully, R. B. 2018, AJ, 156, 105
Asahina, Y., & Ohsuga, K. 2024, ApJ, 973, 45
Astropy Collaboration, Price-Whelan, A. M., Sipőcz, B. M., et al. 2018, AJ, 156, 123
Astropy Collaboration, Robitaille, T. P., Tollerud, E. J., et al. 2013, A&A, 558, A33
Berghea, C. T., Johnson, M. C., Secrest, N. J., et al. 2020, ApJ, 896, 117
Beuchert, T., Middleton, M. J., Soria, R., et al. 2024, MNRAS, 534, 645
Blair, W. P., Fesen, R. A., & Schlegel, E. M. 2001, AJ, 121, 1497
Blundell, K. M., & Bowler, M. G. 2004, ApJL, 616, L159
Corbel, S., Coriat, M., Brocksopp, C., et al. 2013, MNRAS, 428, 2500
Cseh, D., Corbel, S., Kaaret, P., et al. 2012, ApJ, 749, 17
Cseh, D., Kaaret, P., Corbel, S., et al. 2014, MNRAS, 439, L1
Cseh, D., Miller-Jones, J. C. A., Jonker, P. G., et al. 2015b, MNRAS, 452, 24
Cseh, D., Webb, N. A., Godet, O., et al. 2015a, MNRAS, 446, 3268
Deller, A. T., Brisken, W. F., Phillips, C. J., et al. 2011, PASP, 123, 275
Dhawan, V., Mirabel, I. F., & Rodríguez, L. F. 2000, ApJ, 543, 373
Dubner, G. M., Holdaway, M., Goss, W. M., & Mirabel, I. F. 1998, AJ, 116, 1842
Fabrika, S. 2004, ASPRv, 12, 1

Fabrika, S., Ueda, Y., Vinokurov, A., Sholukhova, O., & Shidatsu, M. 2015, NatPh, 11, 551
Fabrika, S. N., Atapin, K. E., Vinokurov, A. S., & Sholukhova, O. N. 2021, AstBu, 76, 6
Fender, R. P., Belloni, T. M., & Gallo, E. 2004, MNRAS, 355, 1105
Fender, R. P., Homan, J., & Belloni, T. M. 2009, MNRAS, 396, 1370
Ferrarese, L., Ford, H. C., Huchra, J., et al. 2000, ApJS, 128, 431
Gladstone, J. C., Roberts, T. P., & Done, C. 2009, MNRAS, 397, 1836
Greisen, E. W. 2003, ASSL, 285, 109
Heida, M., Jonker, P. G., Torres, M. A. P., et al. 2016, MNRAS, 459, 771
Jeffrey, R. M., Blundell, K. M., Trushkin, S. A., & Mioduszewski, A. J. 2016, MNRAS, 461, 312
Kaaret, P., Feng, H., & Roberts, T. P. 2017, ARA&A, 55, 303
Kaaret, P., Ward, M. J., & Zezas, A. 2004, MNRAS, 351, L83
Keimpema, A., Kettenis, M. M., Pogrebenko, S. V., et al. 2015, ExA, 39, 259
King, A., Lasota, J.-P., & Middleton, M. 2023, NewAR, 96, 101672
Koljonen, K. I. I., & Russell, D. M. 2019, ApJ, 871, 26
Lacey, C., Duric, N., & Goss, W. M. 1997, ApJS, 109, 417
Lacy, M., Baum, S. A., Chandler, C. J., et al. 2020, PASP, 132, 035001
Lang, C. C., Kaaret, P., Corbel, S., & Mercer, A. 2007, ApJ, 666, 79
Lara-López, M. A., Zinchenko, I. A., Pilyugin, L. S., et al. 2021, ApJ, 906, 42
Lehmann, I., Becker, T., Fabrika, S., et al. 2005, A&A, 431, 847
Lin, L. C.-C., Hu, C.-P., Li, K.-L., et al. 2020, MNRAS, 491, 5682
Madhusudhan, N., Rappaport, S., Podsiadlowski, P., & Nelson, L. 2008, ApJ, 688, 1235
Marlowe, H., Kaaret, P., Lang, C., et al. 2014, MNRAS, 444, 642
Meier, D. L. 1982, ApJ, 256, 681
Merloni, A., Heinz, S., & di Matteo, T. 2003, MNRAS, 345, 1057
Mezcua, M., Farrell, S. A., Gladstone, J. C., & Lobanov, A. P. 2013, MNRAS, 436, 1546
Mezcua, M., & Lobanov, A. P. 2011, AN, 332, 379
Middleton, M. J., Miller-Jones, J. C. A., Markoff, S., et al. 2013, Natur, 493, 187
Middleton, M. J., Walton, D. J., Alston, W., et al. 2021, MNRAS, 506, 1045
Middleton, M. J., Walton, D. J., Fabian, A., et al. 2015, MNRAS, 454, 3134
Migliari, S., Fender, R. P., Blundell, K. M., Méndez, M., & van der Klis, M. 2005, MNRAS, 358, 860
Miller, N. A., Mushotzky, R. F., & Neff, S. G. 2005, ApJL, 623, L109
Miller-Jones, J. C. A., Jonker, P. G., Dhawan, V., et al. 2009, ApJL, 706, L230
Mineo, S., Gilfanov, M., & Sunyaev, R. 2012, MNRAS, 419, 2095
Motch, C., Pakull, M. W., Soria, R., Grisé, F., & Pietrzyński, G. 2014, Natur, 514, 198
Pakull, M. W., & Mirioni, L. 2002, arXiv:astro-ph/0202488
Pakull, M. W., Soria, R., & Motch, C. 2010, Natur, 466, 209
Pannuti, T. G., Duric, N., Lacey, C. K., et al. 2002, ApJ, 565, 966
Panurach, T., Dage, K. C., Urquhart, R., et al. 2024, ApJ, 977, 211
Paragi, Z., van der Horst, A. J., Belloni, T., et al. 2013, MNRAS, 432, 1319
Pinto, C., Middleton, M. J., & Fabian, A. C. 2016, Natur, 533, 64
Pinto, C., & Walton, D. J. 2023, in High-Resolution X-ray Spectroscopy, ed. C. Bambi & J. Jiang (Springer), 345
Poutanen, J., Lipunova, G., Fabrika, S., Butkevich, A. G., & Abolmasov, P. 2007, MNRAS, 377, 1187
Qiu, Y., & Feng, H. 2021, ApJ, 906, 36
Roberts, T. P., Goad, M. R., Ward, M. J., & Warwick, R. S. 2003, MNRAS, 342, 709
Saha, A., Claver, J., & Hoessel, J. G. 2002, AJ, 124, 839
Saha, A., Thim, F., Tammann, G. A., Reindl, B., & Sandage, A. 2006, ApJS, 165, 108
Sądowski, A., & Narayan, R. 2015, MNRAS, 453, 3213
Shepherd, M. C., Pearson, T. J., & Taylor, G. B. 1994, BAAS, 26, 987
Soria, R., Pakull, M. W., Broderick, J. W., Corbel, S., & Motch, C. 2010, MNRAS, 409, 541
Soria, R., Pakull, M. W., Motch, C., et al. 2021, MNRAS, 501, 1644
Stirling, A. M., Spencer, R. E., Cawthorne, T. V., & Paragi, Z. 2004, MNRAS, 354, 1239
Stirling, A. M., Spencer, R. E., de la Force, C. J., et al. 2001, MNRAS, 327, 1273
Su, Y., Zhou, X., Yang, J., et al. 2018, ApJ, 863, 103
Urquhart, R., Soria, R., Johnston, H. M., et al. 2018, 475, 3561
Urquhart, R., Soria, R., Pakull, M. W., et al. 2019, MNRAS, 482, 2389
van Dyk, S. D., Sramek, R. A., Weiler, K. W., Hyman, S. D., & Virden, R. E. 1994, ApJL, 425, L77
Webb, N., Cseh, D., Lenc, E., et al. 2012, Sci, 337, 554
Williams-Baldwin, D., Muxlow, T. W. B., Lucatelli, G., & Beswick, R. J. 2025, MNRAS, 540, 239
Zhang, Y., Feng, H., Wang, A., & Soria, R. 2026, ApJ, 997, 285
Zhou, C., Feng, H., & Bian, F. 2023, ApJ, 947, 52
Zhou, Y., Feng, H., Ho, L. C., & Yao, Y. 2019, ApJ, 871, 115